THE JOURNAL OF PHYSICAL CHEMISTRY C
A JOURNAL OF THE AMERICAN CHEMICAL SOCIETY

pubs.acs.org/JPCC

Article

Amine Structure Governs Corrosion Rates of Copper Catalysts in Electrochemical Reactive Capture of CO_2

Published as part of The Journal of Physical Chemistry C special issue "Degradation of Electrochemical Materials in Energy Conversion and Storage".

Jounghwan Choi, Avishek Banerjee, R. Dominic Ross, Zisheng Zhang, Shawn Chiu, Robert L. Sacci, Gabriel M. Veith, Christopher Hahn, Anastassia N. Alexandrova,* and Carlos G. Morales-Guio*

Cite This: *J. Phys. Chem. C* 2025, 129, 16009−16019

Read Online

ACCESS | Metrics & More | Article Recommendations | Supporting Information

ABSTRACT: Reactive capture of CO_2 (RCC) offers an integrated approach that combines CO_2 capture with its direct electrochemical conversion, eliminating the need for CO_2 release from the capture agent. By avoiding the pH, pressure, and temperature swings required for the release step, RCC has the potential to reduce both energy consumption and capital costs compared to the conventional sequential process of CO_2 capture, release, concentration, and conversion. Amines, widely used in industrial CO_2 capture, face challenges in RCC systems due to their incompatibility with transition metal catalysts as well as their tendency to promote electrode corrosion and parasitic hydrogen evolution. Identifying suitable combinations of amines and catalysts is therefore critical to enabling integrated CO_2 capture and conversion. This work systematically investigates the performance of four primary and four secondary amines for RCC on polycrystalline Cu catalysts. Among the eight tested amines, only dimethylamine showed no measurable Cu corrosion near the open circuit potential. In contrast, ammonia, methylamine, ethylamine, monoethanolamine, diethylamine, diethanolamine, and piperazine all induced Cu corrosion. Corrosion rates correlate with the pK_a and steric hindrance of the amines, highlighting key parameters for catalyst−amine codesign. Grand canonical DFT calculations indicate a correlation between the adsorption strength of protonated amines, their pK_a, and the extent of Cu corrosion, suggesting that both the surface binding of protonated amines and the lability of their protons play critical roles in corrosion acceleration near open circuit potentials. These finding suggest that amines with high pK_a values and weak binding of their protonated forms to Cu surfaces are preferred, as they offer better corrosion resistance.

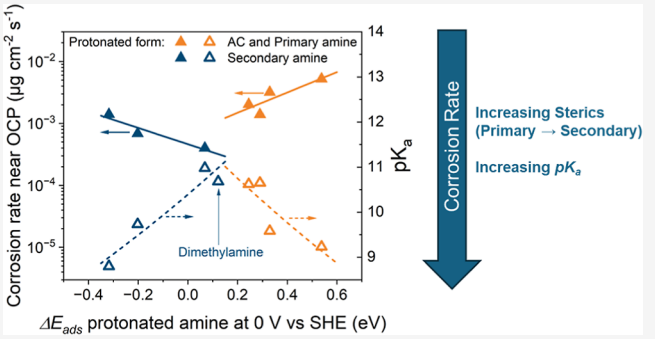

INTRODUCTION

The rising concentration of atmospheric CO_2, now exceeding 420 ppm, poses a critical threat to the environment highlighting the urgency of reaching net-zero CO_2 emissions by 2050 to keep global warming within safe limits.[1−3] Electrochemical CO_2 reduction (CO_2R) has emerged as a promising strategy for mitigating climate change.[4−6] However, current CO_2R systems rely on purified, pressurized CO_2 feedstocks, typically derived from postcombustion capture using amine-based solvents. In conventional CO_2 capture systems, amines cyclically absorb CO_2 at high-pressure and low-temperature and are regenerated at low-pressure and high-temperature. This cycle incurs high energy and capital costs due to thermal, pressure, and pH swings that destroy exergy and reduce process efficiency.[7−9] To enable CO_2 capture and utilization at global scales, more integrated and energy-efficient approaches are required.

Reactive capture of CO_2 (RCC) offers a promising alternative by directly coupling CO_2 capture with electrochemical conversion, thereby eliminating the need for the energy-intensive steps of CO_2 separation, compression and transport.[2,8−17] Comparative studies between conventional CO_2R systems and RCC suggest that direct amine−CO_2 electrolysis can deliver up to 40% energy savings by avoiding CO_2 thermal desorption,[14] with additional process integration benefits leading to a projected 12% reduction in operating costs and a 6.1% decrease in the levelized cost of CO production.[15] However, the successful deployment of RCC

Received: May 9, 2025
Revised: August 15, 2025
Accepted: August 21, 2025
Published: August 28, 2025

https://doi.org/10.1021/acs.jpcc.5c03178
J. Phys. Chem. C 2025, 129, 16009−16019

faces a major challenge: the incompatibility between conventional amine-based capture agents and key electrocatalysts, particularly copper (Cu), which is essential for producing multicarbon products. Understanding and overcoming this incompatibility is critical to realizing the full energy and cost benefits of RCC.

Amines remain the most utilized CO_2 capture agents and are increasingly explored in RCC applications.[15,18−28] For instance, Shen et al. demonstrated that in Ag-based RCC systems, freely dissolved CO_2 serves as the primary carbon source for electrochemical reduction, while amine−CO_2 adducts are likely to contribute as a secondary carbon source only at highly negative applied potentials.[21] Similarly, Leverick et al. investigated the pH-dependent speciation of CO_2 in monoethanolamine capture solutions and confirmed that dissolved CO_2 dominates electrochemical activity on Ag catalysts.[22] Other studies have investigated how temperature, catalyst porosity, and cation concentration affect CO production in RCC systems.[23,27] However, across these studies, the amine−CO_2 adduct is not the principal electroactive species, underscoring the need for catalyst-capture agent pairs that can directly activate these adducts for reduction. While numerous studies have underscored the potential for the use of amines in RCC systems, the electrochemical upgrading of amines has primarily focused on the use of silver catalysts.[18,21−23,26] Cu catalysts, however, are of paramount importance in CO_2 reduction research due to their unique selectivity for the selective formation of high-value C_{2+} products, for which insights from silver catalysts do not necessarily apply.[4,29,30] Although the use of Cu catalysts in RCC applications has begun to be explored, hydrogen remains the predominant product under aqueous conditions, and the physicochemical principles that drive changes in the activity and stability of Cu during electrochemical RCC remain poorly understood.[31−33]

Recent work from our group showed that Cu and Sn corrode during the electrochemical upgrading of an ammonia carbon capture solution near the open circuit potential, while metals like Ag, Au, and Ti are immune to corrosion under the same conditions.[31] While Cu corrosion in the presence of amines, and other N-containing molecules has been studied in the context of electrochemical corrosion and metal protection, its implications for RCC applications are less well understood.[34−40] The introduction of CO_2 in amine-based RCC solutions further complicates the study of electrochemical corrosion as noninnocent carbamates and carbonates modify local pH values and speciation. Strmčnik et al. showed that copper dissolution in CO_2-free ammonia solutions has a reaction order of 2 with respect to ammonia and proposed a two-step passivation mechanism involving Cu_2O formation as the primary corrosion pathway at potentials near the onset for Cu-oxidation.[35] On the other hand, Kumar et al. found that amino acids inhibit copper corrosion by forming stable chemical bonds with copper surfaces through multidentate bonding via amine ($-NH_2$) and carboxyl ($-COOH$) groups.[40] Their DFT study showed glutathione to have the highest corrosion inhibition efficiency among the amino acids tested, and this aligned with experimental trends that suggest that adsorption and passivation of surfaces is more effective for molecules with stronger electron donation through the lone pairs on the N- and O atoms in the amino acids.[40] Surface adsorption and chemical bond formation between amine capture agents and the Cu surface, however, may be detrimental in RCC electrochemistry as this could interfere with the catalysis. The role of CO_2-adducts in determining catalysis and stability under applied potential is not understood. Compounding the challenge, Cu surfaces are known to restructure dynamically under CO_2R conditions,[41−44] and such restructuring may be further influenced by amine−metal interactions and CO_2 adduct−metal interactions.[45] Therefore, rational codesign of amine capture agents and Cu catalysts for RCC demands a detailed understanding of how amines, carbamates, and carbonates interact with the catalyst surface under operating conditions.

While various components of RCC systems have been studied in isolation, a fundamental challenge lies in the codesign of amine capture agents and Cu catalysts. This design space is constrained by two principal issues: (i) amine-induced corrosion of Cu surfaces, and (ii) promotion of the parasitic hydrogen evolution reaction (HER) promoted by amines and their CO_2 adducts. These phenomena reduce catalyst durability and suppress the formation of carbon-based products, limiting the efficacy of RCC. Despite growing interest in amine-based RCC, there is a lack of mechanistic insight into how specific molecular properties, particularly acidity (pK_a) and steric hindrance, govern Cu corrosion and catalytic performance under operating conditions.

In this work, we address this gap by systematically evaluating how the molecular structure of eight commonly used amines (four primary and four secondary) affects corrosion rates and electrocatalytic behavior on polycrystalline Cu under RCC conditions. The selected amines span a range of steric and electronic properties, including ammonia and alkyl amines, as well as monoethanolamine, diethanolamine, and piperazine that represent industrial amines for CO_2 capture. Using electrochemical quartz crystal microbalance (eQCM) measurements, we monitor Cu mass changes as a function of potential and time. We computed binding energy descriptors to systematically model all eight amines, aiming to provide a practical framework to probe the complex environment of the RCC system and enable rapid screening of suitable sorbents for RCC. This approach has been successful in correlating theoretical calculations with experimental observations in CO_2R,[46−48] but it still remains a challenge in RCC. Through the use of grand canonical DFT calculations we identify the binding energy of adsorption of the protonated amine as a predictive descriptor of corrosion behavior, and propose structure−function relations that can inform future codesign strategies for more effective and stable RCC systems.

METHODS

Catalyst Preparation. For eQCM corrosion research, Cu films were deposited via sputtering onto Au-coated quartz crystals. Oak Ridge National Laboratory supplied all the sputtered films for experimental use. The metal targets were 2 in. diameter discs (Kurt Lesker, 99.999%). During sputtering, the target-to-substrate distance was maintained at 7.5 cm. The vacuum chamber was pumped down to a base pressure of 5×10^{-7} Torr for at least 3 h prior to introducing Ar gas (99.999%, AirGas). The system was then stabilized at a pressure of 20 mTorr, and plasma was ignited and sustained using a 20 W DC power source. Each sample film had a thickness of 300 nm.

In the RCE experiments, Cu cylinder electrodes (99.99% purity, 12 mm outer diameter, 8 mm length, from Pine Research Instrumentation) with a geometric area of 3 cm^2 were initially polished using 600 grit sandpaper, followed by a

https://doi.org/10.1021/acs.jpcc.5c03178
J. Phys. Chem. C 2025, 129, 16009−16019

fine polish with 0.05 μm alumina on a microcloth pad. After sonication in distilled water, the Cu was electropolished in concentrated *o*-phosphoric acid (≥85% HPLC grade, Fisher Chemical) at 1.6 V versus a Cu counter electrode for 5 min.

Electrolyte Preparation. Different amine concentrations were used in this work and these are indicated in the caption next to each experimental result. 4.0 M aqueous stock solutions of all the amines were first prepared for the CO_2 loading experiments, except for ammonia and some of the dimethyl amine solutions where the starting amine forms were ammonium carbamate and dimethylammonium dimethylcarbamate salts. The captured solution was then diluted to 0.5 M for all the eQCM corrosion studies and to 0.2 M for the electrochemical characterization studies in our RCC cell.

The 4.0 M solutions for CO_2 loading were prepared by diluting the as-received amines (methylamine (CH_3NH_2 40 wt % solution in water, Sigma-Aldrich), ethylamine ($CH_3CH_2NH_2$ 70 wt % solution in water, Sigma-Aldrich), monoethanolamine ($NH_2CH_2CH_2OH$ 98%, Sigma-Aldrich), dimethylamine ($(CH_3)_2NH$ 40 wt % in water, Sigma-Aldrich), diethylamine ($(C_2H_5)_2NH$ 99.5%, Sigma-Aldrich), diethanolamine ($(CH_2CH_2OH)_2NH$ 99%, Sigma-Aldrich), piperazine ($C_4H_{10}N_2$ 99%, Sigma-Aldrich), and pyridine (C_5H_5N 99.8%, Sigma-Aldrich)) in water. Potassium perchlorate ($KClO_4$ 99.99%, Thermo Fisher) and potassium hydroxide (KOH 99.97%, Sigma-Aldrich) were also added as the supporting electrolyte. 2 M ammonium carbamate and dimethylammonium dimethylcarbamate electrolytes (4 mol of amines per L) were prepared by dissolving ammonium carbamate ($NH_4-NH_2CO_2$ 98%, Thermo Fisher), dimethylammonium dimethylcarbamate ($(CH_3)_2NH-(CH_3)_2NCOOH$, Sigma-Aldrich) in a potassium perchlorate and potassium hydroxide electrolyte. Dimethylammonium dimethylcarbamate ($(CH_3)_2NH-(CH_3)_2NCOOH$, Thermo Fisher) was additionally used in separate contamination control studies. The concentration of $KClO_4$ and KOH in all solutions were 0.099 and 0.001 M, respectively. The stock solution was freshly prepared before each experiment, after which CO_2 loading experiments were conducted using these solutions.

CO_2 Loading Experiments. All CO_2 loading experiments were conducted in a 150 mL RDE/RRDE glass cell from Pine Research, featuring a center port (24/25) and four side ports (14/20). One side port was replaced with a dual-port gas inlet (Pine Research) to allow gas sparging into the solution. The remaining ports were sealed with PTFE stoppers (Pine Research). The capture agent solution for CO_2 loading was prepared as outlined in the Electrolyte Preparation section, with a liquid volume of 50 mL used in all experiments. Mass and pH were recorded every 10 min during CO_2 loading until the solution reached saturation, defined as the point when no further net CO_2 mass change and pH change were observed. CO_2 was bubbled through the solution at a rate of 70 sccm under atmospheric pressure. It is noted that the formation of solids and precipitates was not observed in any of our CO_2 loading experiments at our operating conditions of 1 atm and 293 K. Evaporative losses were accounted for by purging Ar gas at 70 sccm and measuring mass loss to consider solvent evaporation. Net CO_2 loading was determined by subtracting the mass loss due to solvent evaporation (from Ar bubbling) from the mass change recorded during CO_2 loading (from CO_2 bubbling) as described below.

$$\alpha = \text{net } CO_2 \text{ loading (mol of } CO_2\text{/mol of amine)}$$

$$= [(\text{mass change from } CO_2 \text{ bubbling} - \text{mass change from Ar bubbling})/44]/[\text{mol of capture agent used}]$$

All the CO_2-loaded amine solutions were purged with argon at 50 sccm for 15 min to remove as much dissolved CO_2 as possible before doing electrochemistry. We note that the calculated CO_2 loading does not reflect the exact CO_2 loading under the operational conditions of the RCE and eQCM tests, as a dilution step of amine solution is required during experiments. The actual CO_2 loading during RCE experiments can be determined through the VLE model based on the measured pH and the partial pressure of CO_2 in the cell's headspace during electrochemical testing. In this work CO_2-loaded amine solutions refers to solutions after CO_2 loading at 1 atm and Ar purging for 15 min. A schematic workflow is provided in the Supporting Information (Figure S17). The uniqueness of the CO_2 loading method used here is not related to the CO_2 capture process itself, but to being able to track mass changes and pH changes during both the CO_2 capture and reduction process and identify the active species getting reduced during RCC.

Corrosion Experiments. All electrochemical stability tests were conducted on fresh Cu films sputtered onto Au-coated eQCM crystals. A commercially available eQCM cell from Gamry was used, employing the same setup as in previous study.[31] This setup with the eQCM cell enabled a systematic analysis of corrosion on Cu in various amine solutions, dependent on the applied potential. Corrosion rates were measured in two stages. First, 7 mL of a 0.099 M potassium perchlorate and 0.001 M potassium hydroxide solution was added to the eQCM cell. Once a stable potential was achieved with this supporting electrolyte at the designated current, 1 mL of amine stock solution (prepared as outlined in the Electrolyte Preparation section) was introduced to reach a final amine concentration of 0.5 M. Corrosion rates were measured after the amine solution was added to the eQCM cell. Each corrosion rate experiment was repeated at least once.

Electrochemical Characterization. The RCC experiments were carried out using an RCE cell which is a device previously used by our group to determine the contributions from dissolved CO_2 and CO_2-capture agent adduct for RCC on transition metals. A 76 mL volume of supporting electrolyte was introduced into the RCE cell, and a constant current of -4 μA cm^{-2} was applied under a constant flow of Ar at 20 sccm. Next, 4 mL of the amine stock solution was then added to prevent the Cu electrode from being exposed to amine species at open circuit potential. Once the potential and CO_2 partial pressure stabilized following the addition of the amine, chronopotentiometry was conducted at a constant current of -12 mA cm^{-2} with continuous Ar flow. In each experiment, five gas GC injections were obtained, with the average of the final four injections used for analysis and representation in all figures. Additionally, the partial pressure of CO_2 in the cell headspace was measured with each GC injection to determine the equilibrium concentration of dissolved CO_2 with the captured CO_2 in the bulk electrolyte. Diluting the stock solution to 0.2 M for the RCE experiments allows us to measure the CO_2 peak in the GC and consequently quantify the amount of dissolved CO_2 present in the system, the CO_2 loading, and the speciation using VLE models. Higher concentration amine solutions hold more CO_2 into it, resulting

https://doi.org/10.1021/acs.jpcc.5c03178
J. Phys. Chem. C 2025, 129, 16009−16019

in the overloading of the GC FID detector hindering the CO_2 peak quantification. We have tracked the pH after dilution to confirm that the CO_2 loading does not change in this process (Figure S7). Electrochemical impedance spectroscopy (EIS) was performed, and the uncompensated resistance was determined from the real component of the resistance measured at high frequencies ($f \geq 100$ kHz). This resistance was subsequently used to correct all chronopotentiometry data.

Product Characterization. An online GC is used to detect and quantify gaseous products during the experiment. Injections from the cell headspace were taken every 20 min. A sampling cycle includes a 14 min phase for separation and quantification of products followed by a 6 min cooling interval. Details on the procedure for product quantification are given in our previous report.[31]

NMR Analysis. All NMR spectra were collected with Bruker NEO 600 spectrometer. NMR samples were prepared by mixing 700 μL of the sample with 105 μL of a D_2O/TMSP-d_4 solution as an internal standard. The internal standard solution was prepared by mixing 1 mL of deuterium oxide (D_2O, 99.9%, EMD Millipore) with 15 mg of 3-(trimethylsilyl)propionic-2,2,3,3-d_4 acid, sodium salt (TMSP-d_4, 98+ atom % D, Sigma-Aldrich).

Physical Characterization. Scanning electron microscopy (ZEISS Supra 40VP SEM) was used to analyze the morphology and microstructures of the sputtered Cu films before and after corrosion experiments with ammonium carbamate.

Slab Model. The Cu(111) surface was modeled with a cell dimension of about 15 Å × 15 Å. The bottom two layers were constrained as the rigid interior, and everything else was allowed to relax as the catalytic interface. A vacuum layer of 40 Å was added under the periodic boundary condition.

DFT Methods. DFT calculations were performed using the VASP program (version 5.4.4), with the RPBE functional,[49] DFT-D3 dispersion correction,[50] and PBE_PAW pseudopotentials.[51] The cutoff energy for the plane-wave basis set was set to 400 eV, and Gaussian smearing with a width of 0.1 eV was used. The convergence criterion for electronic minimization and geometry optimization were set to 10^{-6} eV and 0.02 eV/Å, respectively. Only the gamma k-point sampling in the reciprocal space of the Brillouin zone was used due to the large supercell used.

Grand Canonical DFT (GCDFT). To calculate the adsorption energy as a function of electrochemical potential, the catalytic interface of the electrode was treated as a grand canonical ensemble of electrons. Different amounts of electrons are used to shift the work function and sample the free energy surface. The surface charging technique[52] was used to calculate the potential-dependent, grand canonical free energy of the surface, ΔG, which is given by

$$\Delta G(U^{\mathrm{VAC}}) = \Delta E^{\mathrm{elec}}(U^{\mathrm{VAC}}) - q(U^{\mathrm{VAC}})FU^{\mathrm{VAC}}$$

where $\Delta E^{\mathrm{elec}}(U^{\mathrm{VAC}})$ is the electronic energy at potential U^{VAC}, the vacuum scale potential of the electrode, q is the number of supplied electrons to the system, and F is the Faraday constant. The system's work function was computed relative to the initial charge of the adsorbate. By treating the catalytic interface as an ideal capacitor, ΔG can be approximated by

$$\Delta G(U^{\mathrm{VAC}}) \approx \Delta E^{\mathrm{elec}}(U_0^{\mathrm{VAC}}) - \frac{1}{2}C(U^{\mathrm{VAC}} - U_0^{\mathrm{VAC}})^2$$

where U_0^{VAC} is the vacuum scale zero charge potential, and C is the effective capacitance. U^{VAC} can be converted to the potential with respect to the standard hydrogen electrode, U^{SHE} by

$$U^{\mathrm{SHE}} = U^{\mathrm{VAC}} - 4.44$$

VASPsol,[53] a linearized Poisson–Boltzmann implicit solvation model, was used to represent the polarizable electrolyte region. The dielectric constant of water was used and set to 78.4. The Debye screening length was set to 3 Å, which corresponds to 1 M concentration of electrolytes evaluated by

$$\lambda \approx \frac{3}{\sqrt{I}}\ \text{Å}$$

where I is the ionic strength in M.[52] The slabs were symmetrized to avoid asymmetric potential in the polarized solvation region, and the thickness of the solvent was set to 90 Å.

Adsorption Energies Calculations. The adsorption geometry was first sampled and optimized at different binding sites. The GCDFT free energy of adsorption of the most stable configurations were calculated by

$$\Delta G_{\mathrm{ad}}(U^{\mathrm{SHE}}) = \Delta G(U^{\mathrm{SHE}}; *\mathrm{ad}) - \Delta G(U^{\mathrm{SHE}}; *) - E(\mathrm{ad})$$

where * denotes the electrode–electrolyte interface and ad denotes the adsorbate.

RESULTS AND DISCUSSION

To investigate the interaction between Cu catalysts and CO_2-loaded amines at the electrode surface, we measured Cu corrosion rates in the presence of eight amine-based capture agents using an electrochemical quartz crystal microbalance (eQCM). The tested solutions included CO_2-loaded ammonia, methylamine, ethylamine, monoethanolamine, dimethylamine, diethylamine, diethanolamine, and piperazine. The ammonia carbon capture solution was prepared by dissolving ammonium carbamate (AC) in water, while all other amine capture solutions were prepared by loading CO_2 into the free amine forms prior to the eQCM experiments. CO_2 loading experiments were performed by flowing 70 sccm of CO_2 into each amine solution. During CO_2 loading, the mass and pH changes were tracked until CO_2 saturation was reached (Figures S1 and S2). The amine solutions take around 100 min to be fully loaded with CO_2 and to reach equilibrium with a partial pressure of CO_2 of 1 atm (Figure S1). Larger mass changes correspond to higher CO_2 loadings. The pH of the solutions quickly decreases from highly alkaline values (pH of 11.5–13.5, depending on the amine) during the first few minutes of CO_2 loading (Figure S2) and eventually reaches an equilibrium pH value of between 7 and 9 after 100 min. The final pH value is that of the amine solution in equilibrium with a partial pressure of CO_2 of 1 atm at room temperature.[27] Figure S3 shows the net CO_2 loading value (α) of amines after the CO_2 loading experiment. Here, α corresponds to the mol of captured CO_2 per mol of amine. CO_2 loading values range between 0.5 and 0.9 for the different amines and correspond to the maximum loading values achievable under a CO_2 partial pressure of 1 atm at room temperature. After loading, all solutions were purged with Ar at 50 sccm for 15 min to remove as much dissolved CO_2 as possible before doing electrochemistry. This does not mean that all the dissolved CO_2 is removed, as the solution rapidly equilibrates to release CO_2

https://doi.org/10.1021/acs.jpcc.5c03178
J. Phys. Chem. C 2025, 129, 16009–16019

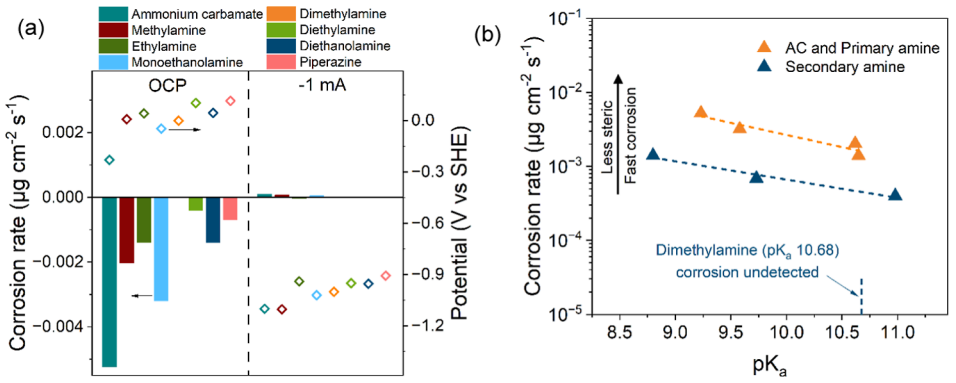

Figure 1. (a) The corrosion rates (bars) and measured potentials (dots) of sputtered Cu films after the exposure to CO_2-loaded 0.5 M amine solutions near the open circuit potential and under a current density of −1 mA cm^{-2}. (b) The corrosion rate values versus the pK_a for investigated amines. The corrosion rate of dimethylamine, showing no detectable corrosion behavior, is not plotted.

when the partial pressure of CO_2 in the headspace is decreased. We have previously shown that the quantification of CO_2 in the headspace of the electrochemical cells under Ar flow and the pH of the solution can be used to estimate the concentration of dissolved CO_2 in solution during electrochemistry.[27] In addition to determining the concentration of dissolved CO_2, the use of vapor−liquid equilibrium (VLE) models can also be used to determine speciation. Figure S4 shows the change in mass and pH as a function of time for an experiment where Ar was purged for 90 min after CO_2 loading in a 4 M MEA solution. The pH and CO_2 loading reach a new quasi-steady state as the capture solution starts to stabilize with the low partial pressure of CO_2 under the Ar flow in the cell overhead. While the pH increases and the loading decreases, the VLE model tracks the change in speciation and allow us to start to close the gap in relating activity and performance to speciation in the RCC electrolyte under dynamic operation.

During the eQCM experiments, we have measured the initial mass change rates for polycrystalline Cu thin films in the presence of each amine at a constant current of −1 μA cm^{-2} (near open circuit potential, OCP) and −1 mA cm^{-2} (representing electrocatalytic reduction conditions). The potential and mass change rates during these experiments are shown in Figure 1a. In our previous work,[31] we observed that the addition of ammonium carbamate to a solution of potassium perchlorate electrolyte led to the corrosion of the Cu film near OCP, and we also observed the formation of a coordination complex between Cu ions and ammonia molecules in the bulk of the solution. Optical and SEM images of the sputtered Cu films before and after corrosion with ammonium carbamate are shown in Figure S22. Similarly, Cu exhibited corrosion behavior from all the tested amines, except for dimethylamine. Corrosion rates range from approximately −0.0004 to −0.005 μg cm^{-2} s^{-1} for the sputtered Cu thin films near OCP. The time-dependent changes in mass and applied potential for each amine under the two selected constant current conditions are shown in Figures S5 and S6. At the low currents, near the open circuit potential, the potential measured ranges from 0.15 to −0.3 V vs SHE. At the most cathodic currents of −1 mA cm^{-2}, the potential measured ranges from −0.9 to −1.2 V vs SHE. While Cu corrosion is generally observed at conditions near OCP, a slight increase in the mass was observed for all the amines under the more cathodic potential and could be indicative of the adsorption of species in solution and strong interactions between the Cu surface and the amine capture agents. At the most negative potentials and under high current densities and local pH values, amines could compete with electrolyte cations for space in the double layer, particularly if there are favorable adsorption interactions that could drive amines to bind and linger for longer at the catalyst surface.

From the experimental observations summarized in Figure 1a, we can identify three principal (though to some extent interdependent) characteristics of amine capture agents that impact Cu corrosion behavior. These are (i) steric effects, (ii) the acidity of the amine's conjugate acid, and (iii) the nucleophilicity of nitrogen within the amine structure. The observed corrosion behavior arises from the combined action of these effects.

First, less steric hindrance in amines leads to accelerated Cu corrosion. As illustrated in Figure 1b, the corrosion rates of secondary amines (blue triangles) are lower than those of ammonia and primary amines (orange triangles). This indicates that sterically hindered amines physically limit access to the electrode surface and impede electron donation which can eventually slow down the corrosion reaction of the Cu catalyst near the open circuit potential.[54,55]

Second, corrosion rates seem to increase as the pK_a of the amine decreases. Prior to the addition of the amines to the supporting electrolyte solution (consisting of 0.099 M $KClO_4$ + 0.001 M KOH) in the eQCM cell, a constant current of −1 μA cm^{-2} was applied to the Cu film to bring the Cu surface to as close as possible to its metallic state. However, due to the aqueous electrolyte, the potential measured at these low cathodic currents near the open circuit potential correspond to those where Cu is thermodynamically expected to exist as Cu_2O. This is based on the Pourbaix diagram of Cu in water at 25 °C, where for an aqueous solution with a pH of 10.2 the thermodynamically stable form at potentials between 0.0 and 0.2 V vs SHE is Cu_2O.[56] Upon the addition of the amine solution, the measured pH in the eQCM cell drops and is lower than the respective pK_a values of the amines (Figure S7), and thus a high concentration of protonated amines is expected in the solution. The pK_a values of the amines used in the stability tests and the pH of the corresponding amine solutions are shown in Figure S7. Upon the introduction of the amine solution under these conditions, protonated amines can react with the surface oxide layer near the open circuit potential, facilitating the generation of Cu^{2+} ions.[34] Free amines coordinate with Cu^{2+} ions due to their high Lewis basicity, leading to the solvation of the Cu−amine complex.[35] Therefore, amines with lower pK_a values, and thus stronger

https://doi.org/10.1021/acs.jpcc.5c03178
J. Phys. Chem. C 2025, 129, 16009−16019

conjugate acids, are more efficient at driving acid−base reactions with the oxide surface, resulting in accelerated Cu corrosion. This leads to more positive potentials being required to sustain a constant current density in the eQCM experiments upon the addition of the CO_2-loaded amine solutions (Figures S5 and S6).

Lastly, strong nucleophilicity of nitrogen in the amine structure increases the reactivity of the amines for corrosion. For example, we observe that dimethylamine, with a slightly lower pK_a and less sterically hindered nitrogen atom than diethylamine, did not induce Cu corrosion in our eQCM experiments. This, we hypothesize, is due to the fact that the larger alkyl group of diethylamine imparts a greater electron-donating inductive effect on the nitrogen atom, thus increasing the nucleophilic attack of the diethylamine on the Cu atoms compared to the dimethylamine. Steric factors play a considerably greater role in the nucleophilicity for secondary amines than for primary amines.[57] The stronger electron-donating substituents stabilize the initial adsorption of amines on the Cu surface by increasing their reactivity to the amine, thereby facilitating the formation of Cu−amine complexes.[45]

At the more cathodic potentials, eQCM measurements did not reveal any corrosion behavior on Cu films under all tested amine solutions. In the potential range between −0.9 V and −1.4 V vs SHE, Cu remains in its metallic state, rendering it highly immune to corrosion.[56] This explains why, following the initial mass step jump upon amine addition, the mass change rate of Cu remains near zero under reductive conditions. However, the absence of corrosion in our eQCM results does not necessarily imply that Cu is completely unreactive with the amines. Recently, Guan et al. demonstrated that amine ligands in solution can directly chemisorb onto the Cu electrode, coordinate with the metal center, and induce the rearrangement of the Cu surface by extracting Cu as adatoms in low coordination sites. These amine ligands can further stabilize surface copper−ligand complexes even under negative potential conditions.[45] Therefore, the initial mass increase immediately after amine addition could potentially be explained by the binding of amine ligands on the Cu surface. This interaction can alter the electronic structure of the catalyst, influencing how the Cu catalyst reacts with intermediates, shifts reaction pathways, or even partially blocks active sites on the Cu surface due to amine ligands. Having established the corrosion behavior of Cu in CO_2-loaded amine solutions, we next investigated whether these surface interactions also influence the electrocatalytic performance of Cu for CO_2 reduction under RCC conditions.

The same amines tested with the eQCM for stability studies were investigated for the electrochemical reduction of captured CO_2 at a constant current density of −12 mA cm^{-2} under constant Ar flow. The electrochemical reduction of potassium bicarbonate electrolyte under Ar flow was used as a reference. Figure 2 shows the Faradaic efficiencies observed for the different capture agents on Cu electrodes. The sum of the Faradaic efficiencies is higher than 95% and the only observed product is hydrogen for all cases when using 0.2 M of the CO_2-loaded amine solvents, while 0.21% of CH_4 was detected from 0.2 M bicarbonate electrolyte. Detailed descriptions of products and Faradaic efficiencies are shown in Table S1 in the Supporting Information. In our observation, the applied potentials are a function of HER kinetics which is a more facile reaction than CO_2R or RCC. Some amines have a higher propensity to form H_2 than others, and this depends on the

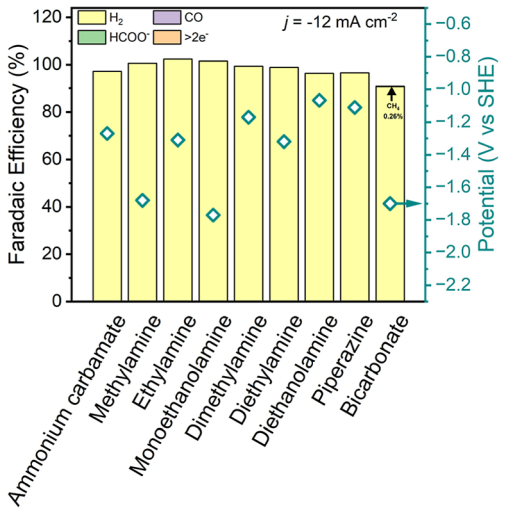

Figure 2. Faradaic efficiency for direct electrochemical reduction of 0.2 M amine solution electrolytes under Ar flow at 20 sccm. The right *y*-axis shows surface potential vs SHE. RCE experimental conditions: The rotation rate of the cylinder electrode in the RCE cell is 800 rpm, the constant current is −12 mA cm^{-2}, and the electrochemical cell temperature is 20 °C.

intrinsic pK_a of the amine (i.e., the dissociation kinetics of the amines in aqueous solutions), and the sterics of the amine (i.e., how hindered the molecule is to undergo reduction near the surface of the electrode). It is hard to determine which factor plays a bigger role in HER as there are other species, like bicarbonate and water, that are present simultaneously in the solution and also contribute to HER. Furthermore, the speciation as discussed in this paper is a function of CO_2 loading, pH, temperature, and pressure. Therefore, more detailed study by varying the pH, partial pressure and amine concentrations is needed to elucidate the exact mechanism of HER in RCC systems.

As established in our previous research, the carbon products generated under RCC conditions arise from the electrochemical reduction of dissolved CO_2 rather than from the reduction of amine−CO_2 adducts, so the amount of carbon product is proportional to the partial pressure of CO_2.[21] It is noted that while Cu can produce CH_4 from bicarbonate, it does not generate carbon-based products in amine solutions even when the CO_2 partial pressures and consequently the amounts of dissolved CO_2 are comparable or higher than those in the bicarbonate solution (Figure S8). Although the reduction of dissolved CO_2 is thermodynamically favorable under RCC operating conditions, the complete absence of carbon products on Cu is noteworthy despite the high loading of CO_2 in the system (0.5 to 0.9 mol of CO_2 per mol of amine). GC data from a blank injection taken before the start of electrolysis (when the j = −4 μA cm^{-2}, near OCP), and an injection during RCC electrolysis at j = −12 mA cm^{-2} are shown in Figures S9 and S10 for each of the amines in Figure 2. For comparison, the GC data for bicarbonate is shown in Figure S11 where methane is observed as the minor product, while the GC peak is well above the detection limit. The complete absence of any carbon product on the Cu catalyst may result from strong interactions between the amine ligands and the Cu surface, which could deactivate or block active sites responsible for CO_2 reduction on the Cu catalyst. Further

https://doi.org/10.1021/acs.jpcc.5c03178
J. Phys. Chem. C 2025, 129, 16009−16019

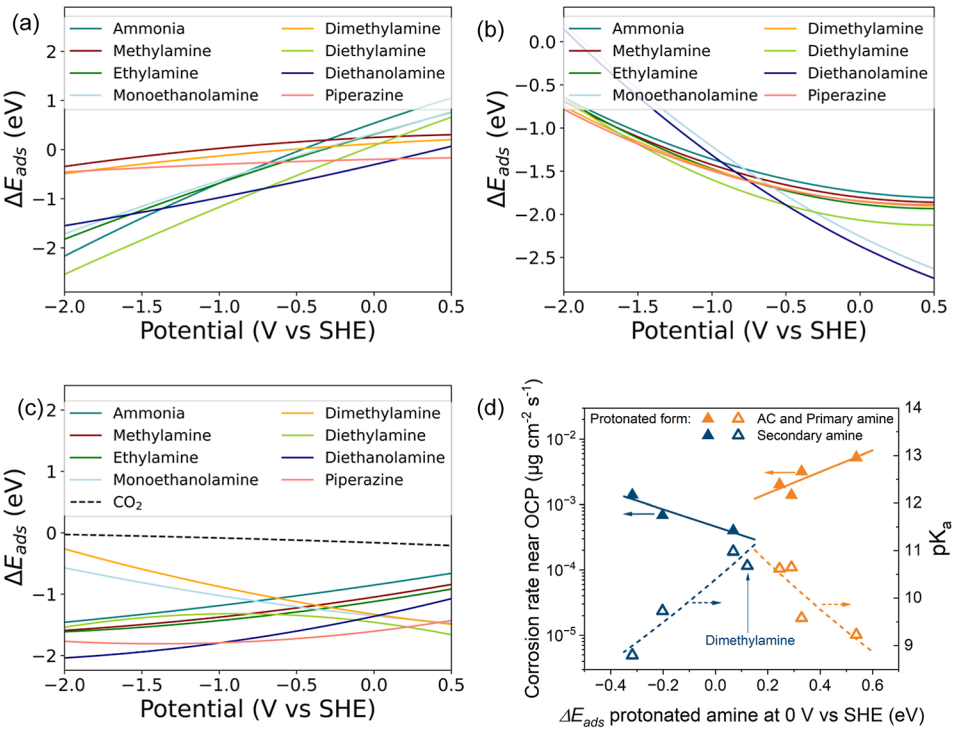

Figure 3. Adsorption energies, ΔE_{ads}, of (a) the protonated form, (b) the CO_2 adduct, and (c) the neutral form, as well as CO_2, of the investigated amines on Cu as a function of electrochemical potential. (d) Experimental corrosion rate near OCP (left axis), and pK_a values (right axis) of primary and secondary amines as a function of the calculated adsorption energy of the protonated form at 0 V vs SHE.

investigation is required to fully elucidate this interaction and its impact on RCC systems.

Recently, methane has been reported as a product of carbamate reduction on Au supported catalysts.[28] CH_4 production on bare gold was attributed to single atom impurity sites, while CO selectivity was preferred when metal impurities were removed using a chelating agent, indicating that CH_4 formation can be driven by the presence of impurities while not being the result of direct carbamate electroreduction.

Initial experiments on the reduction of 0.2 M dimethylammonium dimethylcarbamate solution using Cu electrodes in our RCE cell also showed traces of methane with Faradaic efficiencies (F.E.) for CH_4 of about 0.035%. Although these amounts only correspond to 1−2 ppm of CH_4 in the headspace of the cell, the mechanistic implications of CH_4 formation coinciding with the lack of corrosion of the Cu surface were interesting, as these both were unique to dimethylamine. Further investigation, however, revealed that the partial current densities of CH_4 were independent from the applied potentials (Figure S12) and that any catalytic activity for CO_2 reduction could be eventually attributed to metal impurities in the carbamate reagent. Using ICP−MS measurements on the electrolyte solution we observed that commercially available dimethylcarbamate solutions contained high levels of Fe, Ca, and Pt impurities which could be the potential reasons for the trace amounts of CH_4 that is produced (Table S2). To verify this, we used dimethylamine solution and loaded it with CO_2 by bubbling it into the solution at 1 atm (Figure S13). We conducted the same electrochemical experiments on this prepared solution and did not see any CH_4 production as shown in Figure S13, despite having nominally the same major speciation in the solution as that of the 0.2 M dimethylammonium dimethylcarbamate electrolyte (Figure S14). The only product observed was H_2.

To further investigate the role of the impurities identified in Table S2 (Fe, Ca, and Pt), we intentionally introduced Fe and Ca into the CO_2-loaded dimethylamine solution to assess their impact on CH_4 production (Figure S15). However, we were unable to detect any CH_4, and experiments with the intentional addition of Pt were not pursued as these could cause a contamination of our experimental setup. Rather than trying to identify if Pt was the source of the low activity for CH_4, we performed electrochemical reduction experiments using dimethylcarbamate from an alternative supplier under the same conditions as the experiment where CH_4 was initially observed, yet, no CH_4 production was detected (Figure S16). This suggests that the CH_4 observed was due to the presence of impurities in the as-purchased carbamate salt and not the reduction of the carbamate on Cu. These findings reinforce that trace methane formation is not an intrinsic feature of dimethylamine-based RCC chemistry, and highlight the importance of using high-purity reagents when evaluating CO_2 electroreduction performance in RCC systems. More detailed discussion on the role of impurities in RCC is presented in the Supporting Information.

To gain theoretical insights into the experimentally observed corrosion behavior, we performed grand canonical DFT (GCDFT) calculations to determine the potential-dependent adsorption energies of three species: the protonated form, the CO_2 adduct, and the neutral form of each amine. As shown in our previous work,[31] common descriptors used in CO_2R are inadequate in rationalizing the activity and stability in RCC. Therefore, we have calculated the binding energy specifically related to the speciation of the amine to rationalize the corrosion behavior observed in the experiments. The system's work function was computed relative to the initial charge of the adsorbate, as described in the Methods section, and the optimized geometries are provided in Figures S18−S20.

https://doi.org/10.1021/acs.jpcc.5c03178
J. Phys. Chem. C 2025, 129, 16009−16019

Since the adsorption energy represents the thermodynamics of the binding of an isolated adsorbate when it is present at the interface, the bulk speciation at different applied potentials should also be considered to determine the availability of species at the interface. Given that the equilibrium pH (Figure S2) is lower than the pK_a of all studied amines (Figure 1b), a substantial fraction of each amine is protonated under RCC conditions. These protonated species dominate near the open circuit potential, while under more negative, cathodic potentials, the dominant amine species at the catalyst−electrolyte interface may shift to either the neutral amine or the CO_2 adduct,[26] depending on buffering kinetics and transport rates under the local high pH conditions. Thus, protonated amines are key to understanding corrosion near OCP, whereas the neutral and CO_2-adduct forms are more relevant for catalysis and electrode restructuring.

At more negative potentials relevant to electrocatalysis, all protonated amines show favorable adsorption on Cu. However, under these cathodic conditions and under the flow of current, local pH increases at the Cu surface, shifting the dominant amine species toward either the neutral form or the CO_2 adduct, depending on the relative rates of transport of species in and out of the double-layer as well as the rate of the electrolyte and the amine buffering reaction kinetics. At a first approximation, the protonated form of the amine is the most relevant species for understanding corrosion near OCP, while the neutral amine and CO_2 adduct are more relevant for interpreting catalysis and restructuring of electrodes under applied negative potentials.

Figure 3d reveals a correlation between the adsorption energy of the protonated amines, their pK_a, and the experimentally measured corrosion rates. Corrosion resistance is maximized when amines combine high pK_a values (weaker acidity) with moderate adsorption strengths. This balance allows surface protection without enhancing proton-mediated oxide dissolution. Amines with lower pK_a values, in contrast, more readily donate protons that facilitate oxide dissolution and promote Cu dissolution, even if their adsorption is weak. An extended discussion on why dimethylamine showed no measurable Cu corrosion near the open circuit potential is given in the Supporting Information. At the electrocatalytic potential under a current density of −1 mA cm^{-2}, the Cu electrode becomes negatively charged, allowing favorable adsorption of cationic species. Under these conditions, protonated amines can help inhibit corrosion either by forming surface-passivating films (as evidenced by the mass increase observed in the eQCM study), or by stabilizing surface reconstructions that kinetically suppress dissolution. This is consistent with broader literature on corrosion inhibitors, where protonated amines are known to form hydrophobic protective layers that suppress metal dissolution.[58−61] We note that the protonated form of the amine can play an important role in its transport to the surface due to electrostatics, but that once inside of the double layer it could be deprotonated to facilitate HER leaving behind on the surface the neutral form of the amine that has an even more favorable adsorption energy on Cu (Figure 3c).

Again, while protonated amines may inhibit corrosion, they also act as proton donors that enhance the competing hydrogen evolution reaction (HER), as shown in Figure 2. In contrast, the desired reduction species in amine-based RCC, which is the CO_2 adduct, experience increasing electrostatic repulsion at more negative potentials, which reduces their surface accessibility. Consistent with this, Figure 3b shows that the adsorption strength of the CO_2 adducts decreases with increasing negative potential for the investigated amines. Interestingly, monoethanolamine and diethanolamine exhibit strong adsorption near OCP but lose binding strength more rapidly under reducing conditions. This is attributed to the reduced polarizability of the hydroxyl-containing adducts, which limits their stabilization under strongly cathodic bias (Figure S19). These results suggest that rational capture agent design for RCC should consider substituent effects that modulate the adsorption of both protonated amines and CO_2 adducts.

Finally, as shown in Figure 3c, neutral amines bind more strongly to Cu than CO_2 itself. This likely contributes to the lack of carbon products observed experimentally, as amine coverage competes with CO_2 for active sites. Taken together, these findings suggest that amine-based RCC systems face a dual challenge: protonated amines promote HER while blocking corrosion, and free CO_2 and CO_2−amine adducts struggle to compete for adsorption with amines, resulting in the suppression of productive CO_2 reduction. This dual inhibition mechanism provides a molecular rationale for the experimentally observed selectivity toward hydrogen and the absence of carbon-based products in Figure 2. Altogether, these insights demonstrate that the molecular factors that stabilize Cu surfaces against corrosion at negative potentials simultaneously hinder CO_2 activation, underscoring a fundamental constraint in the design of amine-based RCC systems.

CONCLUSIONS

In summary, this study systematically evaluated amine-based capture agents for their potential application in RCC systems using polycrystalline Cu catalysts. Eight primary and secondary amines were assessed for their chemical compatibility with Cu through eQCM analysis and electrocatalytic activity of Cu in these amine solutions was determined using an RCE cell with well-defined transport characteristics. Among the tested amines, only dimethylamine demonstrated compatibility with Cu, showing no corrosion near OCP, whereas all other amines led to catalyst corrosion. The pK_a and steric effects of the amines were found to directly correlate with the corrosion rates of sputtered Cu films. At more cathodic potentials, eQCM revealed no corrosion behavior due to the strong immunity of metallic Cu to corrosion with amines. However, an initial mass increase was observed immediately after amine addition, which is potentially attributed to the binding of amine ligands on the Cu surface that could affect catalysis. To mitigate corrosion in amine-based RCC, the effective adsorption of protonated amines appears crucial, as evidenced by grand canonical DFT calculations that reveal a link between their adsorption strength and the observed corrosion rates. We note that our binding energy descriptor is a simplified model of the complex double layer structure in RCC, and such calculation alone does not determine the dominant species at the interface. Future work should focus on promising sorbent candidates and employ more comprehensive models, such as ab initio molecular dynamics simulation with explicit solvation,[62] that in turn are coupled to continuum reaction-transport models to realistically model the complex local environment in RCC.

In all amine-based capture solutions, parasitic HER dominated the catalysis, with no carbon products observed,

https://doi.org/10.1021/acs.jpcc.5c03178
J. Phys. Chem. C 2025, 129, 16009−16019

whereas CH_4 production was detected in bicarbonate solutions. The absence of carbon products in amine solutions is likely due to the deactivation of Cu catalyst active sites caused by the strong interactions between amine ligands and the Cu surface. These results highlight the challenges limiting the applicability of amine-based capture agents in RCC systems and emphasize the need for further systematic investigation into novel capture agents to advance RCC systems. As a first step, we find that amines with high pK_a values and weak adsorption of their protonated forms should be favored in the design of Cu-based RCC systems. Our results offer mechanistic design rules for amine−catalyst codesign in RCC and identify critical trade-offs between corrosion inhibition and catalytic accessibility. Future efforts should explore alternative families of capture agents that maintain compatibility with active catalyst sites while minimizing parasitic reactions, while also retaining practically useful kinetics for CO_2 capture.

■ ASSOCIATED CONTENT

Supporting Information

The Supporting Information is available free of charge at https://pubs.acs.org/doi/10.1021/acs.jpcc.5c03178.

Additional experimental details, methods, and a schematic of the experimental setup; the computational section includes all methods, structures, and computational parameters (PDF)

■ AUTHOR INFORMATION

Corresponding Authors

Anastassia N. Alexandrova − *Chemistry and Biochemistry Department, University of California, Los Angeles, Los Angeles, California 90095, United States;* orcid.org/0000-0002-3003-1911; Email: ana@chem.ucla.edu

Carlos G. Morales-Guio − *Department of Chemical and Biomolecular Engineering, University of California, Los Angeles, Los Angeles, California 90095, United States;* orcid.org/0000-0002-5840-5591; Email: moralesguio@ucla.edu

Authors

Jounghwan Choi − *Department of Chemical and Biomolecular Engineering, University of California, Los Angeles, Los Angeles, California 90095, United States*

Avishek Banerjee − *Department of Chemical and Biomolecular Engineering, University of California, Los Angeles, Los Angeles, California 90095, United States*

R. Dominic Ross − *Materials Science Division, Lawrence Livermore National Laboratory, Livermore, California 94550, United States;* orcid.org/0000-0002-4192-8230

Zisheng Zhang − *Chemistry and Biochemistry Department, University of California, Los Angeles, Los Angeles, California 90095, United States*

Shawn Chiu − *Chemistry and Biochemistry Department, University of California, Los Angeles, Los Angeles, California 90095, United States;* orcid.org/0009-0000-1927-0455

Robert L. Sacci − *Chemical Sciences Division, Oak Ridge National Laboratory, Oak Ridge, Tennessee 37830, United States;* orcid.org/0000-0002-0073-5221

Gabriel M. Veith − *Chemical Sciences Division, Oak Ridge National Laboratory, Oak Ridge, Tennessee 37830, United States;* orcid.org/0000-0002-5186-4461

Christopher Hahn − *Materials Science Division, Lawrence Livermore National Laboratory, Livermore, California 94550, United States;* orcid.org/0000-0002-2772-6341

Complete contact information is available at: https://pubs.acs.org/10.1021/acs.jpcc.5c03178

Notes

The authors declare no competing financial interest.

■ ACKNOWLEDGMENTS

This work was supported as part of the Center for Closing the Carbon Cycle, an Energy Frontier Research Center funded by the U.S. Department of Energy, Office of Science, Basic Energy Sciences under Award Number DE-SC0023427. Our calculations utilized resources of Perlmutter of the National Energy Research Scientific Computing Center (NERSC) under Contract DE-AC02-05CH11231. Work by R.D.R. and C.H. was conducted under the auspices of the U.S. Department of Energy by Lawrence Livermore National Laboratory under Contract DE-AC52-07NA27344. LLNL release number: LLNL-JRNL-2005401.

■ REFERENCES

(1) Lüthi, D.; Le Floch, M.; Bereiter, B.; Blunier, T.; Barnola, J.-M.; Siegenthaler, U.; Raynaud, D.; Jouzel, J.; Fischer, H.; Kawamura, K.; et al. High-resolution carbon dioxide concentration record 650,000−800,000 years before present. *Nature* **2008**, *453* (7193), 379−382.

(2) Sullivan, I.; Goryachev, A.; Digdaya, I. A.; Li, X.; Atwater, H. A.; Vermaas, D. A.; Xiang, C. Coupling electrochemical CO2 conversion with CO2 capture. *Nat. Catal.* **2021**, *4* (11), 952−958.

(3) Rogelj, J.; Huppmann, D.; Krey, V.; Riahi, K.; Clarke, L.; Gidden, M.; Nicholls, Z.; Meinshausen, M. A new scenario logic for the Paris Agreement long-term temperature goal. *Nature* **2019**, *573* (7774), 357−363.

(4) Nitopi, S.; Bertheussen, E.; Scott, S. B.; Liu, X.; Engstfeld, A. K.; Horch, S.; Seger, B.; Stephens, I. E.; Chan, K.; Hahn, C.; et al. Progress and perspectives of electrochemical CO2 reduction on copper in aqueous electrolyte. *Chem. Rev.* **2019**, *119* (12), 7610−7672.

(5) De Luna, P.; Hahn, C.; Higgins, D.; Jaffer, S. A.; Jaramillo, T. F.; Sargent, E. H. What would it take for renewably powered electrosynthesis to displace petrochemical processes? *Science* **2019**, *364* (6438), No. eaav3506.

(6) Hori, Y. Electrochemical CO2 Reduction on Metal Electrodes Reduction on Metal Electrodes. *Mod. Aspect. Electrochem.* **2008**, *42*, 89−189.

(7) Li, K.; Yu, H.; Feron, P.; Tade, M.; Wardhaugh, L. Technical and energy performance of an advanced, aqueous ammonia-based CO2 capture technology for a 500 MW coal-fired power station. *Environ. Sci. Technol.* **2015**, *49* (16), 10243−10252.

(8) Jerng, S. E.; Gallant, B. M. Electrochemical reduction of CO(2) in the captured state using aqueous or nonaqueous amines. *iScience* **2022**, *25* (7), 104558.

(9) Siegel, R. E.; Pattanayak, S.; Berben, L. A. Reactive capture of CO2: opportunities and challenges. *ACS Catal.* **2023**, *13* (1), 766−784.

(10) Freyman, M. C.; Huang, Z.; Ravikumar, D.; Duoss, E. B.; Li, Y.; Baker, S. E.; Pang, S. H.; Schaidle, J. A. Reactive CO2 capture: A path forward for process integration in carbon management. *Joule* **2023**, *7* (4), 631−651.

(11) Li, M.; Irtem, E.; Iglesias Van Montfort, H.-P.; Abdinejad, M.; Burdyny, T. Energy comparison of sequential and integrated CO2 capture and electrochemical conversion. *Nat. Commun.* **2022**, *13* (1), 5398.

(12) Appel, A. M.; Yang, J. Y. Maximum and Comparative Efficiency Calculations for Integrated Capture and Electrochemical Conversion of CO2. *ACS Energy Lett.* **2024**, *9* (2), 768−770.
(13) Heldebrant, D. J.; Kothandaraman, J.; Dowell, N. M.; Brickett, L. Next steps for solvent-based CO 2 capture; integration of capture, conversion, and mineralisation. *Chem. Sci.* **2022**, *13* (22), 6445−6456.
(14) Xia, Q.; Zhang, K.; Zheng, T.; An, L.; Xia, C.; Zhang, X. Integration of CO2 Capture and Electrochemical Conversion: Focus Review. *ACS Energy Lett.* **2023**, *8* (6), 2840−2857.
(15) Lee, S.; Choi, W.; Kim, J. H.; Park, S.; Hwang, Y. J.; Na, J. Techno-economic analysis and life-cycle assessment of the electrochemical conversion process with captured CO 2 in an amine-based solvent. *Green Chem.* **2023**, *25* (24), 10398−10414.
(16) Gutierrez-Sanchez, O.; De Mot, B.; Daems, N.; Bulut, M.; Vaes, J.; Pant, D.; Breugelmans, T. Electrochemical conversion of CO2 from direct air capture solutions. *Energy Fuels* **2022**, *36* (21), 13115−13123.
(17) Siegel, R. E.; Aceves, M.; Berben, L. A. Direct Electrochemical Conversion of CO2 Sorbent Solution to Formate by a Molecular Iron Catalyst. *ACS Energy Lett.* **2024**, *9*, 2896−2901.
(18) Li, Q.; Qu, T.; Tan, S.; Wang, T.; Ding, Y.; Wang, C.; Zhang, J.; Xiong, Z.; Zhao, Y. Structure−activity relationship of a dual-function amine-based electrolyte for integrated CO2 capture and electrochemical conversion. *Chem. Eng. J.* **2024**, *498*, 155056.
(19) Lee, G.; Li, Y. C.; Kim, J.-Y.; Peng, T.; Nam, D.-H.; Sedighian Rasouli, A.; Li, F.; Luo, M.; Ip, A. H.; Joo, Y.-C.; et al. Electrochemical upgrade of CO2 from amine capture solution. *Nat. Energy* **2021**, *6* (1), 46−53.
(20) Liu, H.; Chen, Y.; Lee, J.; Gu, S.; Li, W. Ammonia-mediated CO2 capture and direct electroreduction to formate. *ACS Energy Lett.* **2022**, *7* (12), 4483−4489.
(21) Shen, K.; Cheng, D.; Reyes-Lopez, E.; Jang, J.; Sautet, P.; Morales-Guio, C. G. On the origin of carbon sources in the electrochemical upgrade of CO2 from carbon capture solutions. *Joule* **2023**, *7* (6), 1260−1276.
(22) Leverick, G.; Bernhardt, E. M.; Ismail, A. I.; Law, J. H.; Arifutzzaman, A.; Aroua, M. K.; Gallant, B. M. Uncovering the active species in amine-mediated CO2 reduction to CO on Ag. *ACS Catal.* **2023**, *13* (18), 12322−12337.
(23) Kowalski, R. M.; Banerjee, A.; Yue, C.; Gracia, S. G.; Cheng, D.; Morales-Guio, C. G.; Sautet, P. Electroreduction of Captured CO2 on Silver Catalysts: Influence of the Capture Agent and Proton Source. *J. Am. Chem. Soc.* **2024**, *146* (30), 20728−20741.
(24) Chen, L.; Li, F.; Zhang, Y.; Bentley, C. L.; Horne, M.; Bond, A. M.; Zhang, J. Electrochemical reduction of carbon dioxide in a monoethanolamine capture medium. *ChemSusChem* **2017**, *10* (20), 4109−4118.
(25) Pérez-Gallent, E.; Vankani, C.; Sánchez-Martínez, C.; Anastasopol, A.; Goetheer, E. Integrating CO2 capture with electrochemical conversion using amine-based capture solvents as electrolytes. *Ind. Eng. Chem. Res.* **2021**, *60* (11), 4269−4278.
(26) Safipour, J.; Weber, A. Z.; Bell, A. T. Detrimental Effects of Monoethanolamine and Other Amine-Based Capture Agents on the Electrochemical Reduction of CO2. *ACS Energy Lett.* **2023**, *8* (12), 5012−5017.
(27) Banerjee, A.; Yue, C.; Choi, J.; Morales-Guio, C. G. Rotating cylinder electrode in reactive CO2 capture: Identifying active C species via transport, VLE models and kinetics. *AIChE J.* **2024**, *70*, No. e18560.
(28) Neves-Garcia, T.; Hasan, M.; Zhu, Q.; Li, J.; Jiang, Z.; Liang, Y.; Wang, H.; Rossi, L. M.; Warburton, R. E.; Baker, L. R. Integrated Carbon Dioxide Capture by Amines and Conversion to Methane on Single-Atom Nickel Catalysts. *J. Am. Chem. Soc.* **2024**, *146* (46), 31633−31646.
(29) Kim, D.; Park, S.; Lee, J.; Chen, Y.; Li, F.; Kim, J.; Bai, Y.; Huang, J. E.; Liu, S.; Jung, E. D.; et al. Acid-Stable Cu Cluster Precatalysts Enable High Energy and Carbon Efficiency in CO(2) Electroreduction. *J. Am. Chem. Soc.* **2024**, *146* (40), 27701−27712.
(30) Hori, Y. I. Electrochemical CO2 reduction on metal electrodes. *Mod. Aspect. Electrochem.* **2008**, *42*, 89−189.
(31) Choi, J.; Chiu, S.; Banerjee, A.; Sacci, R. L.; Veith, G. M.; Stieber, C.; Hahn, C.; Alexandrova, A. N.; Morales-Guio, C. G. Corrosion and enhanced hydrogen evolution in electrochemical reduction of ammonium carbamate on transition metal surfaces. *J. Phys. Chem. Lett.* **2024**, *15* (31), 8007−8017.
(32) Ma, H.; Ibáñez-Alé, E.; Ganganahalli, R.; Pérez-Ramírez, J.; López, N.; Yeo, B. S. Direct Electroreduction of Carbonate to Formate. *J. Am. Chem. Soc.* **2023**, *145* (45), 24707−24716.
(33) Bruggeman, D.; Rothenberg, G.; Garcia, A. Investigating proton shuttling and electrochemical mechanisms of amines in integrated CO2 capture and utilization. *Nat. Commun.* **2024**, *15* (1), 9207.
(34) Aksu, S.; Doyle, F. M. Electrochemistry of copper in aqueous ethylenediamine solutions. *J. Electrochem. Soc.* **2002**, *149* (7), B340.
(35) Strmčnik, D.; Gaberščček, M.; Pihlar, B.; Kočar, D.; Jamnik, J. Copper dissolution in ammonia solutions: identification of the mechanism at low overpotentials. *J. Electrochem. Soc.* **2009**, *156* (7), C222.
(36) Johnson, H.; Leja, J. On the Potential/pH Diagrams of the Cu-NH 3-H 2 O and Zn-NH 3-H 2 O Systems. *J. Electrochem. Soc.* **1965**, *112* (6), 638.
(37) Antonijevic, M.; Petrovic, M. Copper corrosion inhibitors. A review. *Int. J. Electrochem. Sci.* **2008**, *3* (1), 1−28.
(38) Ben Seddik, N.; Achache, M.; Zarki, Y.; Chraka, A.; Bouchta, D.; Raissouni, I. Computational, theoretical and experimental studies of four amino acids as corrosion inhibitors for brass in 3% NaCl medium. *J. Mol. Liq.* **2024**, *397*, 124113.
(39) Zhang, D.-Q.; Cai, Q.-R.; He, X.-M.; Gao, L.-X.; Zhou, G.-D. Inhibition effect of some amino acids on copper corrosion in HCl solution. *Mater. Chem. Phys.* **2008**, *112* (2), 353−358.
(40) Kumar, D.; Jain, N.; Jain, V.; Rai, B. Amino acids as copper corrosion inhibitors: A density functional theory approach. *Appl. Surf. Sci.* **2020**, *514*, 145905.
(41) Simon, G. H.; Kley, C. S.; Roldan Cuenya, B. Potential-Dependent Morphology of Copper Catalysts During CO2 Electroreduction Revealed by In Situ Atomic Force Microscopy. *Angew. Chem., Int. Ed. Engl.* **2021**, *60* (5), 2561−2568.
(42) Zhang, Z.; Gee, W.; Sautet, P.; Alexandrova, A. N. H and CO Co-Induced Roughening of Cu Surface in CO2 Electroreduction Conditions. *J. Am. Chem. Soc.* **2024**, *146* (23), 16119−16127.
(43) Lee, S.; Lin, J.; Farmand, M.; Landers, A.; Feaster, J.; Avilés Acosta, J. E.; Beeman, J.; Ye, Y.; Yano, J.; Mehta, A.; et al. Oxidation state and surface reconstruction of Cu under CO2 reduction conditions from in situ X-ray characterization. *J. Am. Chem. Soc.* **2021**, *143* (2), 588−592.
(44) Yang, Y.; Louisia, S.; Yu, S.; Jin, J.; Roh, I.; Chen, C.; Fonseca Guzman, M. V.; Feijóo, J.; Chen, P.-C.; Wang, H.; et al. Operando studies reveal active Cu nanograins for CO2 electroreduction. *Nature* **2023**, *614* (7947), 262−269.
(45) Guan, Y.; Kümper, J.; Mürtz, S. D.; Kumari, S.; Hausoul, P. J.; Palkovits, R.; Sautet, P. Origin of copper dissolution under electrocatalytic reduction conditions involving amines. *Chem. Sci.* **2024**, *15* (35), 14485−14496.
(46) Peterson, A. A.; Nørskov, J. K. Activity Descriptors for CO2 Electroreduction to Methane on Transition-Metal Catalysts. *J. Phys. Chem. Lett.* **2012**, *3* (2), 251−258.
(47) Todorova, T. K.; Schreiber, M. W.; Fontecave, M. Mechanistic Understanding of CO2 Reduction Reaction (CO2RR) Toward Multicarbon Products by Heterogeneous Copper-Based Catalysts. *ACS Catal.* **2020**, *10* (3), 1754−1768.
(48) Feaster, J. T.; Shi, C.; Cave, E. R.; Hatsukade, T.; Abram, D. N.; Kuhl, K. P.; Hahn, C.; Nørskov, J. K.; Jaramillo, T. F. Understanding Selectivity for the Electrochemical Reduction of Carbon Dioxide to Formic Acid and Carbon Monoxide on Metal Electrodes. *ACS Catal.* **2017**, *7* (7), 4822−4827.
(49) Hammer, B.; Hansen, L. B.; Nørskov, J. K. Improved adsorption energetics within density-functional theory using revised

https://doi.org/10.1021/acs.jpcc.5c03178
J. Phys. Chem. C 2025, 129, 16009−16019

Perdew-Burke-Ernzerhof functionals. *Phys. Rev. B: Condens. Matter Mater. Phys.* **1999**, *59* (11), 7413−7421.
(50) Grimme, S.; Antony, J.; Ehrlich, S.; Krieg, H. A consistent and accurate ab initio parametrization of density functional dispersion correction (DFT-D) for the 94 elements H-Pu. *J. Chem. Phys.* **2010**, *132* (15), 154104.
(51) Kresse, G.; Joubert, D. From ultrasoft pseudopotentials to the projector augmented-wave method. *Phys. Rev. B: Condens. Matter Mater. Phys.* **1999**, *59* (3), 1758−1775.
(52) Steinmann, S. N.; Sautet, P. Assessing a First-Principles Model of an Electrochemical Interface by Comparison with Experiment. *J. Phys. Chem. C* **2016**, *120* (10), 5619−5623.
(53) Mathew, K.; Sundararaman, R.; Letchworth-Weaver, K.; Arias, T. A.; Hennig, R. G. Implicit solvation model for density-functional study of nanocrystal surfaces and reaction pathways. *J. Chem. Phys.* **2014**, *140* (8), 084106.
(54) Goni, L. K.; Yaagoob, I. Y.; Verma, C.; Almustafa, F.; Alobaid, M. Y.; Ali, S. A.; Quraishi, M. A.; Mazumder, M. A. Comparative corrosion inhibition performance of diallyl amine-based cyclo-polymers bearing secondary, tertiary and quaternary nitrogen's motifs in 1 M HCl. *J. Mol. Liq.* **2023**, *375*, 121371.
(55) Tan, B.; Zhang, S.; Qiang, Y.; Guo, L.; Feng, L.; Liao, C.; Xu, Y.; Chen, S. A combined experimental and theoretical study of the inhibition effect of three disulfide-based flavouring agents for copper corrosion in 0.5 M sulfuric acid. *J. Colloid Interface Sci.* **2018**, *526*, 268−280.
(56) Revie, R. W. *Uhlig's Corrosion Handbook*; John Wiley & Sons, 2011.
(57) Brotzel, F.; Chu, Y.; Mayr, H. Nucleophilicities of primary and secondary amines in water. *J. Org. Chem.* **2007**, *72* (10), 3679−3688.
(58) Verma, C.; Quraishi, M. A.; Ebenso, E. E.; Hussain, C. M. Amines as Corrosion Inhibitors. In *Organic Corrosion Inhibitors*; John Wiley & Sons, Inc., 2021; pp 75−94.
(59) Malinowski, S.; Wróbel, M.; Woszuk, A. Quantum Chemical Analysis of the Corrosion Inhibition Potential by Aliphatic Amines. *Materials* **2021**, *14*, 6197.
(60) Jero, D.; Caussé, N.; Pébère, N. Film-forming amines as corrosion inhibitors: a state-of-the-art review. *npj Mater. Degrad.* **2024**, *8* (1), 111.
(61) Zhao, F.; Cui, C.; Dong, S.; Xu, X.; Liu, H. An overview on the corrosion mechanisms and inhibition techniques for amine-based post-combustion carbon capture process. *Sep. Purif. Technol.* **2023**, *304*, 122091.
(62) Chiu, S.; Alexandrova, A. N. Cation Effects on CO2 Delivery to Cu Electrode in Reactive Capture of CO2. *J. Phys. Chem. Lett.* **2025**, *16* (24), 6032−6039.

https://doi.org/10.1021/acs.jpcc.5c03178
J. Phys. Chem. C 2025, 129, 16009−16019